Journal of Engineering Mathematics **37:** 45–64, 2000.

Finite elastic deformations of a thick semicircular fibre-reinforced shell

A. H. ENGLAND
Department of Theoretical Mechanics[*]*, University of Nottingham, Nottingham NG7 2RD, U.K.*

Received 10 February 1998; accepted in revised form 30 September 1998

Abstract. This paper examines the finite plane-strain deformations of a thick semicircular shell which is held fixed along its base and is loaded symmetrically by a rigid plate. The shell is composed of an elastic fibre-reinforced composite material in which the fibres reinforce the shell in the circumferential direction. The composite is assumed to be an 'ideal' material which is inextensible in the fibre direction and is incompressible. The deformations are followed through to the final collapsed state of the shell. An application of these results in the case of an under-inflated vehicle tyre is considered.

Key words: fibre-reinforced, composite material, finite elasticity, tyre.

1. Introduction

This paper considers the finite plane-strain deformation of a long cylinder with a cross-section in the form of a thick semicircular shell (see Figure 1).

The two faces E′E and OO′ of the shell are assumed to be rigidly bonded to a fixed base and the deformation is produced by symmetrically loading the plate P′P, so that it remains parallel to E′O′ and gradually squashes the shell. This may be thought of as the cross-section of a tyre on a wheel of infinite radius where the wheel rims hold the tyre in place across E′E and OO′ and the road surface is P′P. We shall assume the shell undergoes a plane-strain deformation with no extension in the axial direction. The material of the cylindrical shell is assumed to be a fibre-reinforced composite material in which one family of fibres reinforce the shell in the circumferential direction and lie entirely within the cross-section. The effect of the fibres is to make the mechanical response of the composite highly anisotropic with the local fibre direction taking the role of the preferred direction. We shall assume the material is a fibre-reinforced material in which the fibres are continuously distributed throughout the material and deform with it. In general, it is very difficult to solve problems for anisotropic elastic materials. This problem also involves finite deformations and solutions in finite elasticity are often only possible when the material has a simple constitutive relation. However, the idealising assumptions due to Spencer, Rogers and Pipkin that the fibres are inextensible and the material is incompressible permit relatively straightforward solutions to a wide class of problems. Obviously the applicability of this theory is limited to materials for which the extensional modulus in the fibre direction and the bulk modulus are large compared with the in-plane shear modulus of the material, and the mode of deformation is largely a shearing mode.

[*] From 1.8.98 Division of Theoretical Mechanics, School of Mathematical Sciences.

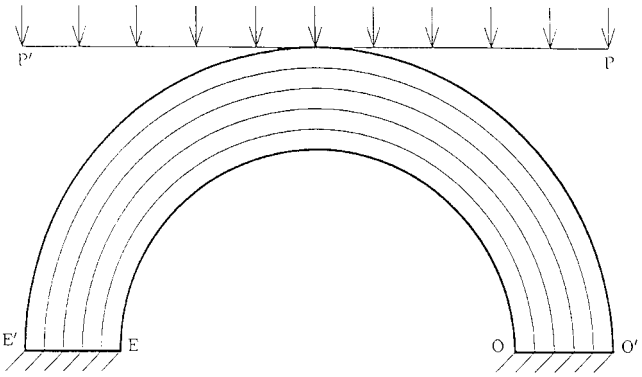

Figure 1. The initial configuration.

The properties of such ideal fibre-reinforced materials have been derived in the monograph by Spencer [1] and in a series of papers by Spencer *et al.* [2], Pipkin and Rogers [3], Pipkin [4], Rogers [5], Spencer [6] and are summarised in Section 2. The important kinematic results governing all finite plane deformations are

1. fibres which are initially parallel remain parallel throughout the deformation;
2. the normal distance between any pair of parallel fibres is the same at all points along that pair, and the fibres remain that same distance apart during the entire deformation history.

This idealised model has permitted Bradford *et al.* [7], England *et al.* [8, 9, 11], Rogers *et al.* [12] and Gregory *et al.* [13], to find the solutions to a series of problems involving large plastic as well as elastic deformations.

The stress in an ideal material is given by

$$\boldsymbol{\sigma} = -p(\boldsymbol{I} - \boldsymbol{aa}) + T\boldsymbol{aa} + S(\boldsymbol{an} + \boldsymbol{na}) + T_{33}\boldsymbol{kk}, \tag{1.1}$$

in dyadic notation, where p and T are the reaction stress components introduced by the constraints of incompressibility and inextensibility, respectively, and S is the shear stress. We denote the current fibre direction by the unit vector **a** and denote the unit vector normal to a fibre in the plane of the deformation by **n**, where **k** is normal to **a** and **n**. The reaction stress T_{33} in the **k** direction maintains the plane-strain configuration.

In this paper we consider a fibre-reinforced material with an elastic matrix in which the shear stress S satisfies the uniaxial stress-strain relation for loading and unloading under simple shear so that

$$S = G\gamma. \tag{1.2}$$

Here G is the elastic shear modulus and it has been shown in the papers cited above that the shear strain γ at a point is related to the angle between the current normal direction **n** and the initial normal direction $\boldsymbol{N}$ at that point, (see Section 2).

Treloar [14] has observed that there is a linear shearing response of the form (1.2) in rubber, even at very large elastic deformations. More recently, Nakajima and Kurashige [15] have experimentally verified the ideal theory for elastic deformations of fibre-reinforced rubbers in the low-load range and proposed a modified constitutive relation with the addition of a cubic term in γ for the shear stress for large elastic deformations.

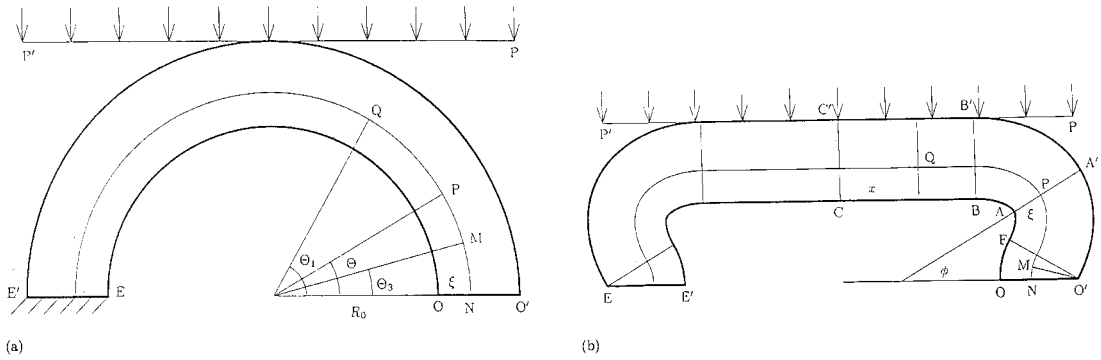

Figure 2. (a) The initial configuration; (b) The deformed configuration.

Rogers and Pipkin [16] have investigated the lateral compression of a fibre-reinforced pressurised hollow tube by two smooth rigid parallel plates. They employ the idealised theory described above and restrict attention to elastic deformations. They briefly interpret their results in terms of the mechanics of vehicle tyres. England and Gregory [17] have extended this work to the loading of elastic-plastic tubes.

In Section 2 we investigate the kinematics of the deformation. The next section describes the elastic deformation of the shell for 'small' loads. In Sections 4 and 5 we describe the progressive flattening of the elastic shell under an increasing load applied to the plates using a minimum-energy method. The final section applies this theory to the deformation of an under-inflated vehicle tyre.

2. Kinematics

We consider a long straight semicircular shell with internal radius R_0 and wall thickness h, and employ the system of polar coordinates (R, Θ) to describe the undeformed body where $R_0 \leqslant R \leqslant R_0 + h$, $0 \leqslant \Theta \leqslant \pi$. (see Figure 2a). We suppose the faces E′E, OO′ of the shell are held fixed and it is squashed by a rigid plate P′P which remains parallel to E′O′ with the normal force on the plate equal to $2W$ per unit length in the axial direction (see Figure 2b). We assume that the deformation is a plane-strain deformation with no extension in the axial direction.

The shell is assumed to be reinforced by a continuous distribution of inextensible fibres that initially lie on the semicircles $R =$ constant. Since the problem is symmetrical about CC′, we will restrict consideration to the right-hand half OCC′O′ of the body.

The kinematic results derived by Pipkin, Rogers and Spencer and summarised in Spencer [6] show that, for plane deformations, the fibres which lie on the circles $R =$ constant deform into a family of parallel curves in which the distance apart of any pair of fibres is conserved. In addition, the orthogonal trajectories of these fibres form straight lines, which we shall refer to as normal lines. Hence, if contact is assumed to be maintained between the section C′B′ of the outer edge fibre and the plate P′P, all fibres under the contact region are straight and that section of the tube deforms into the rectangular region CBB′C′ bounded by the normal lines CC′ and BB′.

We suppose the radial lines $\Theta = 0$ and $\Theta = \pi/2$ map into the normal lines OO′ and CC′, respectively, in the deformed body. Note that these lines contain the same material points in the undeformed and deformed configurations. By symmetry there is no shearing stress across the line CC′. The displacement is zero at all points on OO′. The boundary conditions on the faces OC and O′C′ correspond to the imposition of zero tractions at all points on OC and O′B′ together with a displacement condition along B′C′.

Since the displacement is zero on OO′, as the shell deforms we must assume a fan region forms adjacent to OO′ with its centre at O′ having the (unknown) fan angle $\angle$FO′O$= \alpha$. As the loading W increases we will expect α to increase.

Consider the fibre NMPQ which is at radius $R_0 + \xi$ in the undeformed configuration. This deforms into the fibre NMPQ which is at the distance ξ from the inner boundary OBC of the deformed body. Suppose the normal line through the material point P meets the inner boundary at A, then AP $= \xi$. Let the arclength OA be $s(\phi)$ and denote the angle of inclination of AP to OO′ by ϕ. Then (s, ϕ) form the intrinsic coordinates for the inner surface of shell and, since all fibres are parallel to the inner surface, determine the shape of the shell. If the point P denotes the same material point on the fibre in the undeformed and deformed configurations, since the fibre is inextensible, conservation of the length NP implies

$$(R_0 + \xi)\Theta = (h - \xi)\alpha + \int_{-\alpha}^{\phi} \left(\frac{\mathrm{d}s}{\mathrm{d}\phi} + \xi \right) \mathrm{d}\phi = (h - \xi)\alpha + \xi(\phi + \alpha) + s(\phi) - s(-\alpha)$$

but, $s(-\alpha) = h\alpha$, and hence when P lies in the curved section of the shell

$$(R_0 + \xi)\Theta = s(\phi) + \xi\phi. \tag{2.1}$$

Similarly, if Q lies in the straight section of the shell at length x from CC′, then

$$(R_0 + \xi)\Theta_1 = (R_0 + \xi)\pi/2 - x. \tag{2.2}$$

If M is a point in the fan region OO′F then

$$(R_0 + \xi)\Theta_3 = -(h - \xi)\phi_3, \tag{2.3}$$

where the normal line MO′ is inclined at the (negative) angle ϕ_3 to OO′.

Equations (2.1), (2.2) and (2.3) provide a relation between the current (ξ, ϕ) coordinates of a particle and its initial coordinates $(R_0 + \xi, \Theta)$.

The amount of shear strain γ at a particle can be shown to have the form (see Rogers and Pipkin [16])

$$\gamma = \phi - \Theta, \tag{2.4}$$

where ϕ is the angle of inclination of the normal line through that particle after deformation. Further we note that Θ is the angle of inclination of the normal line in the undeformed configuration, using the result that, by symmetry, the shear strain is zero on each point on CC′.

The shear strain at the point P in the curved section of the shell is then

$$\gamma = \phi - \frac{s(\phi) + \xi\phi}{R_0 + \xi} = \frac{R_0\phi - s(\phi)}{R_0 + \xi} \tag{2.5}$$

and at Q in the straight section of the shell,

$$\gamma = \pi/2 - \Theta_1 = \frac{x}{R_0 + \xi}, \tag{2.6}$$

and at M in the edge fan

$$\gamma = \phi_3 - \theta_3 = \frac{(R_0 + h)\phi_3}{R_0 + \xi}. \tag{2.7}$$

These shear strains may be used to determine the shear stress at each point of the shell.

3. The elastic solution

In the case of purely elastic deformations the shear stress S is specified in terms of the shear strain γ by means of a constitutive relation of the form $S = S(\gamma)$, which we have approximated in this work by the linear shear stress – shear strain relation (1.2) namely

$$S = G\gamma. \tag{3.1}$$

The remaining terms in the constitutive relation (1.1) are the unknown reaction stresses p, T and T_{33} which are determined from the equilibrium equations. It may be shown that there is a sufficient generality in the system so that any kinematically admissible plane-strain deformation is also statically admissible. However, not every kinematically admissible deformation corresponds to a state of minimum potential energy. This criterion has been used by Pipkin [18] and by England, Rogers and Bradford [8] to determine the unique elastic deformation field in certain beam problems.

It will become necessary for us to employ the minimum potential energy technique in due course but, for the time being, we can determine the solution using the more straightforward force resultant method. This solution may also be obtained as a special case of Section 4.

The force resultant method examines the equilibrium of a portion of the body, for example OAA′O′ on Figure 2b. If the reaction forces exerted on the body across OO′ are $W(\alpha)$ upwards and the shear force $X(\alpha)$ to the left, then the component of the resultant force acting along the direction AA′ leads to the equilibrium equation

$$-\int_0^h S(\gamma)\mathrm{d}\xi + W(\alpha)\sin\phi - X(\alpha)\cos\phi = 0 \tag{3.2}$$

for the section OAA′O′. But the shear stress at the height ξ on AA′ has the value

$$S(\gamma) = \frac{G(R_0\phi - s(\phi))}{R_0 + \xi} \tag{3.3}$$

from (2.5), and hence (3.2) reduces to

$$-G(R_0\phi - s(\phi))\log\left(1 + \frac{h}{R_0}\right) + W(\alpha)\sin\phi - X(\alpha)\cos\phi = 0. \tag{3.4}$$

This means that the intrinsic equation of the inner surface FB is given by the equation

$$s(\phi) = R_0\phi - W^*(\alpha)\sin\phi + X^*(\alpha)\cos\phi, \tag{3.5}$$

where the arclength OA is $s(\phi)$ and ϕ is the angle of inclination of AA′ and

$$G^* = G \log\left(1 + \frac{h}{R_0}\right), \qquad W^*(\alpha) = W(\alpha)/G^*, \qquad X^*(\alpha) = X(\alpha)/G^*. \tag{3.6}$$

If the applied load $W(\alpha)$ is specified, then $W^*(\alpha)$ is known, but the fan angle α and the reaction force $X(\alpha)$ remain to be determined from the kinematic conditions on the problem. It turns out to be simpler to specify the fan angle α and to determine the load $W(\alpha)$ and the reaction force $X(\alpha)$ in terms of α and the notation used indicates this dependence on α. Since the arclength $s(\phi)$ is defined by (3.5), at the point F

$$s(-\alpha) = h\alpha, \tag{3.7}$$

which reduces to

$$X^*(\alpha)\cos\,\alpha + W^*(\alpha)\sin\,\alpha = (R_0 + h)\alpha. \tag{3.8}$$

If we denote the length C′B′ of the region of contact by $\ell(\alpha)$ then

$$s(\tfrac{1}{2}\pi) + \ell(\alpha) = R_0\tfrac{1}{2}\pi \tag{3.9}$$

and hence, from (3.5),

$$\ell(\alpha) = W^*(\alpha). \tag{3.10}$$

Since the line OO′ does not move as the body deforms, the x-coordinate of C relative to O has the value $-R_0$. Hence

$$h(1 - \cos\,\alpha) + \int_{-\alpha}^{\pi/2} (-)\sin\,\phi s'(\phi)\mathrm{d}\phi - \ell(\alpha) = -R_0.$$

Performing the integral and using (3.10), we find X^* and W^* satisfy

$$-X^*(\alpha)(\tfrac{1}{2}\pi + \alpha - \sin\,\alpha\,\cos\,\alpha) + W^*(\alpha)(2 - \cos^2\,\alpha) = 2(R_0 + h)(1 - \cos\,\alpha). \tag{3.11}$$

Hence $X^*(\alpha)$ and $W^*(\alpha)$ satisfy the simultaneous equations (3.8) and (3.11), with the solutions

$$\begin{aligned} X^*(\alpha) &= (R_0 + h)[\alpha(2 - \cos^2\,\alpha) - 2\,\sin\,\alpha(1 - \cos\,\alpha)]/D(\alpha), \\ W^*(\alpha) &= (R_0 + h)[2\,\cos\,\alpha(1 - \cos\,\alpha) + \alpha(\tfrac{1}{2}\pi + \alpha - \sin\,\alpha\,\cos\,\alpha)]/D(\alpha), \end{aligned} \tag{3.12}$$

where $D(\alpha) = \cos\,\alpha + (\frac{1}{2}\pi + \alpha)\sin\,\alpha$.

It is simple to confirm that these scaled forces are monotonically increasing functions of α. Similarly, from (3.10), the contact length $\ell(\alpha)$ increases monotonically with α.

The deflection $d(\alpha)$ of inner surface CB of the shell is given by

$$R_0 - h\,\sin\,\alpha - \int_{-\alpha}^{\pi/2} \cos\,\phi s'(\phi)\mathrm{d}\phi \tag{3.13}$$

and hence has the value

$$d(\alpha) = -(R_0 + h)\sin\alpha + \tfrac{1}{2}X^*(\alpha)\cos^2\alpha + \tfrac{1}{2}W^*(\alpha)(\tfrac{1}{2}\pi + \alpha + \sin\alpha\cos\alpha). \qquad (3.14)$$

Again, this may be shown to be a monotonically increasing function of α. Hence from (3.6), (3.12) and (3.14) the load versus deflection curve can be found in terms of the parameter α for this elastic shell and is given later on Figure 5.

Similarly, given the intrinsic equation for the inner surface of the shell (Equation(3.5)), we can evaluate the coordinates of the point A from the integrals

$$x(\phi, \alpha) = h(1 - \cos\alpha) - \int_{-\alpha}^{\phi} \sin\phi s'(\phi)\mathrm{d}\phi$$

$$y(\phi, \alpha) = h\sin\alpha + \int_{-\alpha}^{\phi} \cos\phi s'(\phi)\mathrm{d}\phi$$

and construct the deformed shape of the shell.

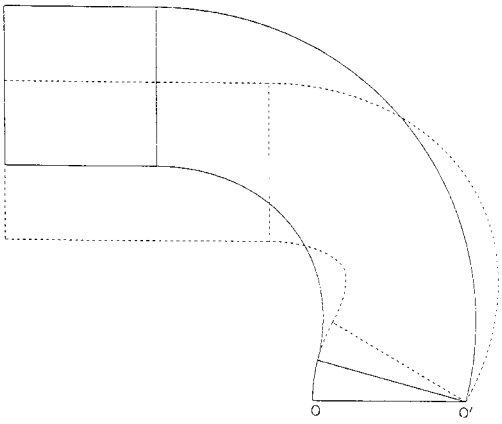

Figure 3. The deformed shapes with $h/R_0 = 0{\cdot}5$ and the fan angles $\frac{1}{12}\pi$ and $\frac{1}{6}\pi$.

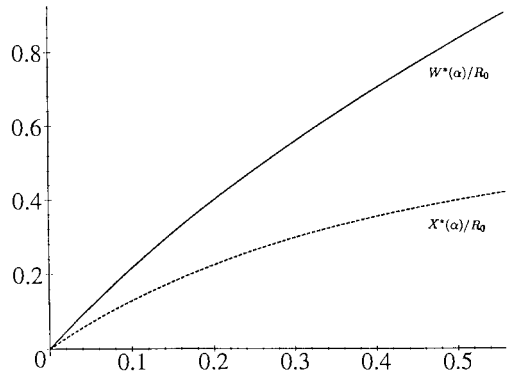

Figure 4. The scaled load $W^*(\alpha)/R_0$ and reaction $X^*(\alpha)/R_0$ as functions of the fan angle α.

The deformed shapes for a thick shell with $h/R_0 = 0{\cdot}5$ are given in Figure 3 when the fan angle α has the value $\frac{1}{12}\pi$ and $\frac{1}{6}\pi$.

It turns out that there is an upper limit on the value of the fan angle α for which these formulae apply. If the angle α is increased, it is found that the curvature of the inner surface drops to zero at some point between F and B, so that the inner surface develops a cusp. The curvature is given by

$$\begin{aligned} s'(\phi) &= R_0 - W^*(\alpha)\cos\phi - X^*(\alpha)\sin\phi \\ &= R_0 - (X^{*2}(\alpha) + W^{*2}(\alpha))^{1/2}\sin(\phi + \varepsilon). \end{aligned}$$

This quantity is first equal to zero when

$$X^{*2}(\alpha) + W^{*2}(\alpha) = R_0^2,$$

which defines the angle $\alpha = \alpha_C$ at which a cusp first appears. The value of α_C depends on the thickness of the shell and takes the value $\alpha_C = 0{\cdot}558$ when $h/R_0 = 0{\cdot}5$, and the value

$\alpha_C = 0{\cdot}8567$ when $h/R_0 = 0{\cdot}1$. The formulae derived in this section only hold over the range $0 \leqslant \alpha \leqslant \alpha_C$.

The scaled load, reaction, and load versus deflection curves for the thick shell case $h/R_0 = 0{\cdot}5$ are given in Figures 4 and 5. The results for the thin shell are given on Figure 12.

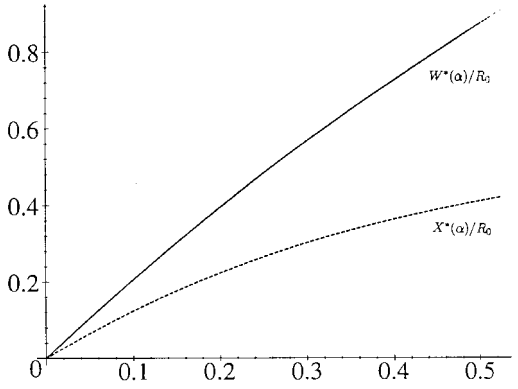

Figure 5. The scaled load $W^*(\alpha)/R_0$ and reaction $X^*(\alpha)/R_0$ as functions of the deflection $/R_0$.

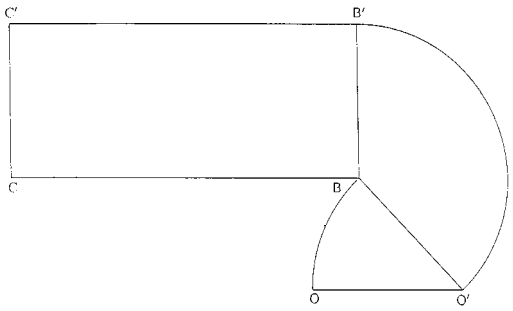

Figure 6. The collapsed configuration for the thick shell $h/R_0 = 0{\cdot}5$.

For a sufficiently thick shell the final 'collapsed' configuration has the form given on Figure 6. If the fan angle is denoted by α_F, then the arclength along the inner surface is

$$h\alpha_F + \ell = R_0 \tfrac{1}{2}\pi \tag{3.15}$$

and the position of C relative to A implies

$$h(1 - \cos\,\alpha_F) - \ell = -R_0. \tag{3.16}$$

These equations have a solution for α_F in the range $0 \leqslant \alpha_F \leqslant \frac{1}{2}\pi$ provided $h/R_0 \geqslant (\pi - 2)/(\pi + 2)$, *i.e.* for shells thicker than $h/R_0 = 0{\cdot}222$.

For shells thinner than this value, the fan angle in the final collapsed condition requires further investigation.

4. The central-fan solution

We have seen that, when the fan angle α reaches the critical value α_C, the radius of curvature of the inner face of the shell drops to zero at one point, indicating the formation of a cusp at that point. This implies that a fan region develops at that point.

Fan regions are a relatively common occurrence in this ideal theory of elasticity, but have normally been found to occur with their centre on a line of symmetry or to emanate from a point force or from points at which the boundary conditions change. To the author's knowledge, this is the first occurrence of a 'free' fan region in which the position of the fan is determined as part of the deformation, although Spencer has investigated the motion of a plastic hinge in an ideal rigid-plastic material and Parker has briefly examined jump conditions across fans in dynamic flexural deformations of a plate (references are given in Spencer [6]).

It is difficult to establish the system of equations which govern the angle and the position of this central fan without employing a more sophisticated approach. To find these equations,

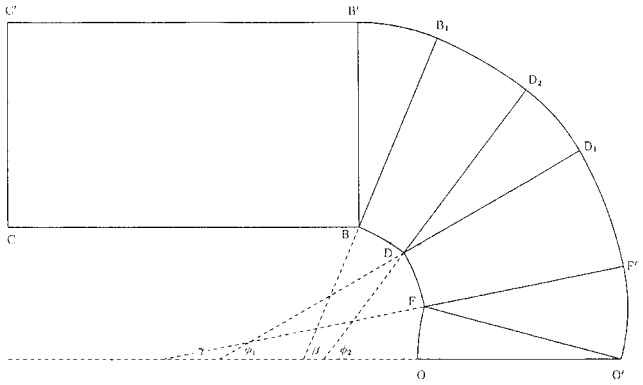

Figure 7. The central and edge fans configuration.

we use a minimum potential energy method which reduces to a problem in the calculus of variations.

Consider the deformation shown in Figure 7. In addition to the central fan located at D we have allowed the possibility of an upper-edge fan located at B and a reversed fan located at F. We denote the angles of inclination of the lines BB_1, DD_2, DD_1 and FF' to the line OO' by β, ϕ_2, ϕ_1 and γ, respectively, so that the fan angle of the upper-edge fan is $\frac{1}{2}\pi - \beta$, the fan angle of the central fan is $\phi_2 - \phi_1$, and that of the reversed fan is $\alpha + \gamma$ (the line FF' coincides with FO' when $\gamma = -\alpha$).

The strain energy in each of the seven sections consists of the integral over the area of $\frac{1}{2}G\gamma^2$, where the strain γ can be found as in (2.5), (2.6) and (2.7). For example, the strain energy in the central fan DD_1D_2 is

$$\begin{aligned} E_4 &= \int_{\phi_1}^{\phi_2}\int_0^h \tfrac{1}{2}G\left[\frac{R_0\phi - s(\phi_1)}{R_0+\xi}\right]^2 \xi\,\mathrm{d}\xi\,\mathrm{d}\phi \\ &= \tfrac{1}{6}G\{[R_0\phi_2 - s(\phi_1)]^3 - [R_0\phi_1 - s(\phi_1)]^3\} f(h/R_0), \end{aligned} \tag{4.1}$$

where

$$f(h/R_0) = \frac{1}{R_0}\log(1 + h/R_0) - \frac{h}{R_0(R_0+h)}. \tag{4.2}$$

Similarly, the strain energy in the curved region $FF'D_1D$ is

$$\begin{aligned} E_3 &= \int_{\gamma}^{\phi_1}\int_0^h \tfrac{1}{2}G\left[\frac{R_0\phi - s(\phi)}{R_0+\xi}\right]^2 [s'(\phi) + \xi]\mathrm{d}\xi\,\mathrm{d}\phi \\ &= \tfrac{1}{2}G\,\log\left(1 + \frac{h}{R_0}\right)\int_{\gamma}^{\phi_1}[s(\phi) - R_0\phi]^2\,\mathrm{d}\phi \\ &\quad -\frac{Gh}{6R_0(R_0+h)}\{[R_0\phi_1 - s(\phi_1)]^3 - [R_0\gamma - s(\gamma)]^3\}, \end{aligned}$$

where $s = s(\phi)$ is the intrinsic equation of the inner face FD.

The potential energy consists of the total strain energy minus the work done by the external force W. This has to be minimised subject to the condition that the x-distance from O to C

should be $-R_0$, which is an integral constraint. If we attach the Lagrange multiplier X to this integral constraint the potential energy function for the system becomes

$$\begin{aligned} &P\{s(\phi), \alpha, \gamma, \phi_1, \phi_2, \beta, X, \ell\} \\ &\quad = E_1 + E_2 + E_3 + E_4 + E_5 + E_6 + E_7 \\ &\qquad + W\left[h \sin \alpha + \int_\gamma^{\phi_1} \cos \phi s'(\phi) \mathrm{d}\phi + \int_{\phi_2}^{\beta} \cos \phi s'(\phi) \mathrm{d}\phi - R_0\right] \\ &\qquad + X\left[\ell - h(1 - \cos \alpha) + \int_\gamma^{\phi_1} \sin \phi s'(\phi) \mathrm{d}\phi + \int_{\phi_2}^{\beta} \sin \phi s'(\phi)\, \mathrm{d}\phi - R_0\right], \end{aligned} \tag{4.3}$$

where E_3 and E_4 have been defined above,

$$\begin{aligned} E_1 &= \frac{G}{6}(R_0 + h)^2 \left\{\frac{h}{R_0} - \log\left(1 + \frac{h}{R_0}\right)\right\} \alpha^3, \\ E_2 &= \frac{G}{6} f\left(\frac{h}{R_0}\right) \{[R_0\gamma - s(\gamma)]^3 + [R_0\alpha + s(\gamma)]^3\}, \\ E_5 &= \frac{G}{2} \log\left(1 + \frac{h}{R_0}\right) \int_{\phi_2}^{\beta} [R_0\phi - s(\phi)]^2 \, \mathrm{d}\phi \\ &\quad - \frac{Gh}{6R_0(R_0 + h)} \{[R_0\beta - s(\beta)]^3 - [R_0\phi_2 - s(\phi_2)]^3\}, \\ E_6 &= \frac{G}{6} f\left(\frac{h}{R_0}\right) \{[R_0 \tfrac{1}{2}\pi - s(\beta)]^3 - [R_0\beta - s(\beta)]^3\}, \\ E_7 &= \frac{Gh\ell^3}{6R_0(R_0 + h)}, \end{aligned} \tag{4.4}$$

where $f(h/R_0)$ is defined in (4.2) and ℓ is the length of the contact region.

The boundary conditions on the arclength $s(\phi)$ are

$$s(\gamma) = h\alpha, \qquad s(\phi_1) = s(\phi_2), \qquad s(\beta) + \ell = R_0 \tfrac{1}{2}\pi, \tag{4.5}$$

together with the integral constraint that the term multiplying X in (4.3) must be zero, namely

$$\ell - h(1 - \cos \alpha) + \left(\int_\gamma^{\phi_1} + \int_{\phi_2}^{\beta}\right) \sin \phi s'(\phi)\, \mathrm{d}\phi = R_0. \tag{4.6}$$

Minimisation of the expression (4.3) is equivalent to solving the calculus of variations problem in which we permit the following independent variations in the function $s(\phi)$ (defined on the intervals $\gamma \leqslant \phi \leqslant \phi_1$ and $\phi_2 \leqslant \phi \leqslant \beta$), together with variations in the geometrical constants $\alpha, \gamma, \phi_1, \phi_2, \beta, \ell$ and in the Lagrange multiplier X, where the load W is held constant:

$$s(\phi) \to s(\phi) + \varepsilon\eta(\phi),$$

$$\alpha \to \alpha + \varepsilon\alpha', \ldots, \quad \beta \to \beta + \varepsilon\beta', \quad \ell \to \ell + \varepsilon\ell', \quad X \to X + \varepsilon X'.$$

On calculating the first variation of (4.3), subject to the boundary conditions (4.5), the following series of equations is obtained.

The Euler–Lagrange equations are identical in the two intervals and reduce to

$$s(\phi) = R\phi - W^* \sin\phi + X^* \cos\phi, \tag{4.7}$$

where

$$W^* = W \Big/ \left[G \log\left(1 + \frac{h}{R_0}\right)\right], \qquad X^* = X \Big/ \left[G \log\left(1 + \frac{h}{R_0}\right)\right]. \tag{4.8}$$

These equations are identical to (3.5) and (3.6) and represent the equilibrium equations for the sectors $\gamma \leqslant \phi \leqslant \phi_1$ and $\phi_2 \leqslant \phi \leqslant \beta$. The Lagrange multiplier X may be identified with the horizontal component of the reaction force along OO′.

The other equations which result from this analysis correspond to one equation for each fan region and the integral constraint. The central-fan equation reduces to

$$s'(\phi_2) - s'(\phi_1) = \tfrac{1}{2}(\phi_2 - \phi_1)[R_0\phi_2 - s(\phi_2) + R_0\phi_1 - s(\phi_1)] \tag{4.9}$$

with similar equations for the upper fan and the reversed fan (with $s'(\frac{1}{2}\pi)$ and $s'(-\alpha)$ being evaluated by substitution in the formula for $s'(\phi)$).

The physical interpretation of this equation is not immediately obvious. The shear strain at a point in the central fan is $(R_0\phi - s(\phi_1))/(R_0 + \xi)$. The integral of this along the fibre from one side of the fan to the other is

$$\tfrac{1}{2}(\phi_2 - \phi_1)[R_0(\phi_2 + \phi_1) - s(\phi_2) - s(\phi_1)]\frac{1}{R_0 + \xi}, \tag{4.10}$$

since $s(\phi_2) = s(\phi_1)$. Hence (4.9) states that the jump in the radius of curvature across the tip of the fan is equal to R_0 multiplied by the integral of the shear strain through the tip ($\xi = 0$) of the fan.

We can also observe that, from (4.7), the intrinsic equation reduces to

$$s''(\phi) = R_0\phi - s(\phi) \tag{4.11}$$

at all points on the inner surface except at the cusp. However, it will be noted that $s(\phi)$ and its derivatives are not defined in $\phi_1 < \phi < \phi_2$. If we assume (4.11) holds in this interval as well, with $s(\phi) = s(\phi_1)$, then integration from ϕ_1 to ϕ_2 yields the Equation (4.9) again.

In terms of X^* and W^* the equations corresponding to the three fans become

$$X^*[(\phi_2 - \phi_1)(\cos\phi_1 + \cos\phi_2) + 2(\sin\phi_1 - \sin\phi_2)] + W^*[-(\phi_2 - \phi_1)(\sin\phi_1 + \sin\phi_2) + 2(\cos\phi_1 - \cos\phi_2)] = 0, \tag{4.12}$$

$$2X^*(\sin\alpha + \sin\gamma) - 2W^*(\cos\alpha - \cos\gamma) = (\alpha + \gamma)[R_0(\alpha - \gamma) + 2h\alpha], \tag{4.13}$$

$$X^*[(\tfrac{1}{2}\pi - \beta)\cos\beta + \sin\beta - 1] - W^*[(\tfrac{1}{2}\pi - \beta)\sin\beta - \cos\beta] = \tfrac{1}{2}R_0(\tfrac{1}{2}\pi - \beta)^2. \tag{4.14}$$

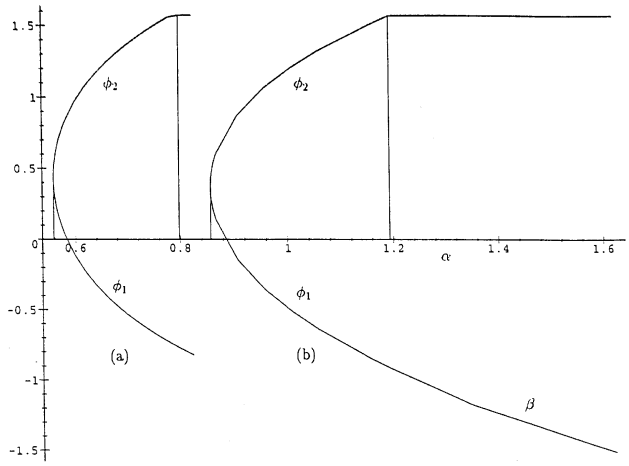

Figure 8. The upper and lower angles of the central fan expressed as a function of α (a) $h/R_0 = 0{\cdot}5$; (b) $h/R_0 = 0{\cdot}1$.

In addition, there are the kinematic relations stemming from the boundary conditions (4.5) and the integral constraint (4.6) which reduce to

$$X^* \cos\gamma - W^* \sin\gamma = h\alpha - R_0\gamma, \tag{4.15}$$

$$X^*(\cos\phi_1 - \cos\phi_2) - W^*(\sin\phi_1 - \sin\phi_2) = R_0(\phi_2 - \phi_1), \tag{4.16}$$

$$\begin{aligned} &X^*[\beta - \phi_2 + \phi_1 - \gamma - \sin\beta\cos\beta + \sin\phi_2\cos\phi_2 - \sin\phi_1\cos\phi_1 \\ &\quad + \sin\gamma\cos\gamma + 2\cos\beta] \\ &-W^*(\cos^2\beta - \cos^2\phi_2 + \cos^2\phi_1 - \cos^2\gamma + 2\sin\beta) \\ &\quad = 2R_0(\tfrac{1}{2}\pi - 1 - \beta - \cos\beta + \cos\phi_2 - \cos\phi_1 + \cos\gamma) - 2h(1 - \cos\alpha). \end{aligned} \tag{4.17}$$

Equations (4.12) to (4.17) correspond to six equations for the six unknowns X^*, W^*, γ, ϕ_1, ϕ_2, β in terms of the parameter α.

In Section 3 we found a central-fan region formed when α exceed the critical angle α_C. Hence, initially, we are looking for solutions of this system of equations in which the upper and reversed fans do not exist, so that $\beta = \frac{1}{2}\pi$ and $\gamma = -\alpha$. In this case (4.13) and (4.14) are satisfied identically and (4.17) is simplified. Numerical investigation of the four remaining equations shows that the central-fan angles ϕ_2 and ϕ_1 change very rapidly with α, when α just exceeds α_C, see Figure 8. As α increases further we see that ϕ_2 increases to $\frac{1}{2}\pi$ before ϕ_1 has decreased to $-\alpha$. This implies that the next region we should examine is that in which the central-fan comes into contact with the edge of the contact region to make a single wide-angle upper fan with the fan angle $\frac{1}{2}\pi - \beta$. We now need to solve the system of Equations (4.14), (4.15) and (4.17) in which $\phi_1 \equiv \phi_2$ and $\gamma = -\alpha$. These solutions are continuous where the fans coincide and, in the case of a thick shell, tend to the collapsed solution of Figure 6 as $\alpha \to \alpha_F$. A reversed fan has not been found so that $\gamma = -\alpha$ throughout.

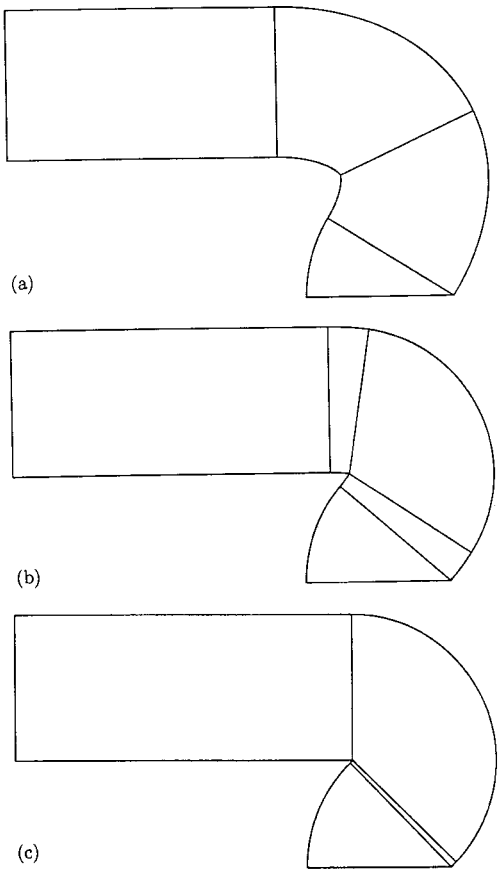

Figure 9. Deformations of the thick shell $h/R_0 = 0{\cdot}5$ (a) the cusp; (b) the central fan; (c) the upper fan.

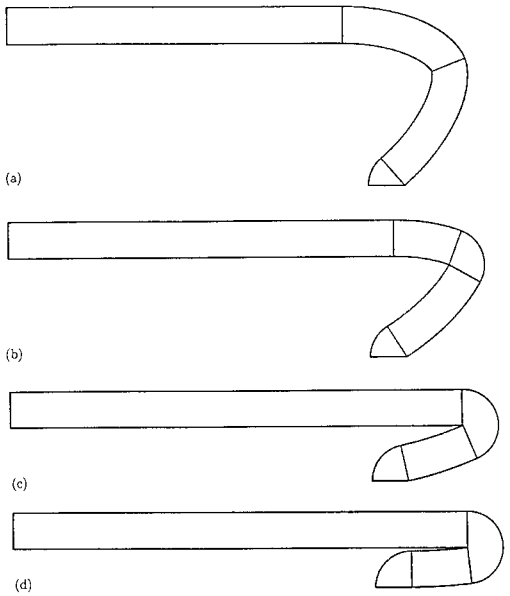

Figure 10. Deformations of the thin shell $h/R_0 = 0{\cdot}1$ (a) the cusp; (b) the central fan; (c) the upper fan; (d) the shape when $\alpha = \frac{1}{2}\pi$.

The corresponding deformations of a thick shell when $\alpha_C \leqslant \alpha < \alpha_F$ are shown in Figure 9. The final collapsed solution is given on Figure 6.

The (quasi-static) dynamics of the deformation field are that, as the load increases, the central-fan region moves down the shell towards O. The contact region increases in length and overtakes the central-fan region to form an upper-fan region, which persists until the collapsed configuration is reached. For the thin shell the upper-fan solution is reached earlier and applies for a wider range of values of α. The corresponding deformations of the thin shell in the range $\alpha_C \leqslant \alpha \leqslant \frac{1}{2}\pi$ are given in Figure 10.

The solution when $\alpha = \frac{1}{2}\pi$ is given in Figure 10d. It will be noted that this is not the final collapsed solution. In fact when $h/R_0 = 0{\cdot}1$, the collapsed solution is reached when $\alpha = \frac{1}{2}\pi + 0{\cdot}0492$ and the deformation is shown on Figure 11. Note that there is contact between the upper and lower parts of this segment of the inner surface at just one point. This is very similar to the run-flat configuration for a vehicle tyre.

It is possible to calculate the load, and the reaction as functions of the fan angle α for these deformations. The results for a thin shell are given in Figure 12. The load versus deflection

curve has a similar shape and is given in Section 6. We see that all curves are monotonically increasing with a slight change in gradient where the nature of the solution changes.

After some considerable manipulation, it may be confirmed that the second variation of the potential energy is positive, indicating that these deformations are stable equilibrium solutions.

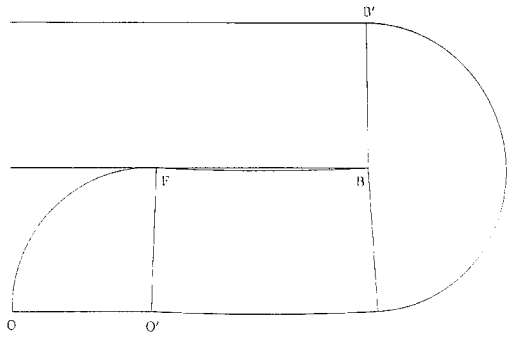

Figure 11. The edge of the collapsed configuration for the thin shell $h/R_0 = 0{\cdot}1$.

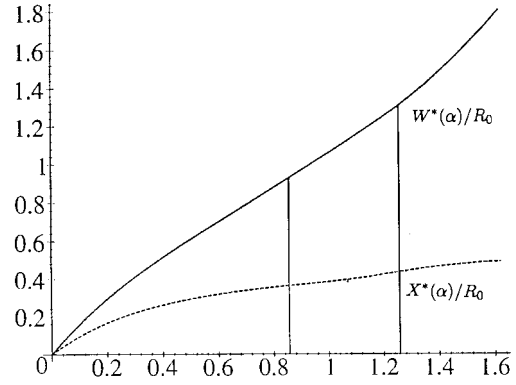

Figure 12. The scaled load $W^*(\alpha)/R_0$ and reaction $X^*(\alpha)/R_0$ as functions of the fan angle α. The central fan and upper fan regions are bounded by vertical lines.

5. The under-inflated tyre problem

The solutions obtained in this paper assume that the internal surface of the shell is unstressed. This is clearly not the case in a vehicle tyre where the internal pressure plays a major part in the stiffness of the tyre structure (nor are tyres semicircular in cross-section). In a sequel to this paper we shall examine the effect of internal pressure and also the effect of a tangential force on the tyre, which will occur when a vehicle is cornering, using the ideal theory to model the deformation. The monograph by French [19] describes the very complex technical problems associated with vehicle tyres and the author is conscious of the sophisticated analytical and numerical methods that have been used to tackle these problems, (see Clark [20]). However, it seems not unreasonable to see if the solutions derived in this paper can be used to generate some quantities of physical interest without too much labour. Given the plane-strain solutions obtained under these zero pressure assumptions, we can obtain estimates of the load-deflation behaviour of the tyre and the size and shape of the contact patch between the tyre and the road. It is convenient to restrict the discussion to the analytical solutions obtain in Section 3, but the extension to the larger deformations is readily carried out.

Suppose a vehicle wheel has a radius R_W to the base of the tyre and that the cross-section of the tyre can be modelled as a semi-circular shell with the internal radius R_0 and thickness h. Consider Figure 13 which represents the deformation of a tyre on the lower half of a wheel. Let us assume the tyre thickness remains equal to h in the deformation. Figure 13 represents the deformation the inner surface of the tyre.

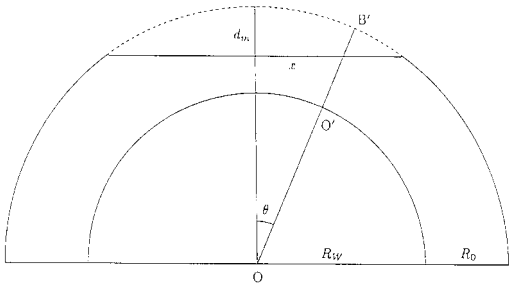

Figure 13. The wheel and tyre.

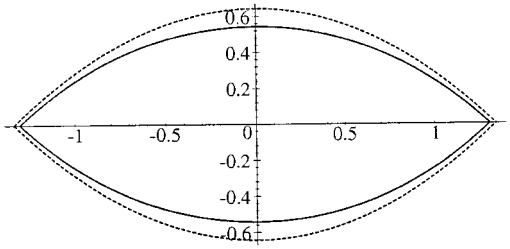

Figure 14. The linearised and exact contact regions when the maximum deflection is $0{\cdot}3R_0$.

Denote the maximum radial deflection of the inner surface by d_m. Then the radial deflection of the radial cross-section OO′B′ of the tyre at distance x from the centre line is equal to

$$d_t(x) = R_W + R_0 - [(R_W + R_0 - d_m)^2 + x^2]^{1/2}. \tag{5.1}$$

and we see $d_t(x) = 0$ when $x = x_m$, where

$$x_m^2 = (R_W + R_0)^2 - (R_W + R_0 - d_m)^2. \tag{5.2}$$

Section 3 provides us with the plane-strain solution for the deflection of the cross-section O′B′ of the tyre, in which the maximum deflection is $d_t(x)$. Note this is a plane-strain solution so that there are out-of-plane reaction stresses which maintain the zero deformation field perpendicular to O′B′. We can assume that this reaction stress field will be approximately equal to that of a neighbouring radial section and hence can approximate the deformation and stress field in the tyre by the plane-strain field in each radial section of the tyre. In fact, since radial ply tyres are also reinforced in the circumferential direction around the wheel, this assumption may not be too unreasonable. Hence, for a given value of d_m, we can evaluate the deflection $d_t(x)$, calculate the fan angle $\alpha = \alpha(x)$ for the deformation of that cross-section O′B′, find the corresponding load $2W^*\{\alpha(x)\}$ carried by that cross-section and find the width $2l\{\alpha(x)\}$ of the contact region.

It is easier to formulate the calculation in terms of the fan angle α, noting that at the edge $x = x_m$ of the contact region the fan angle is zero, and that α reaches its maximum along $x = 0$ where the value $\alpha = \alpha_m$ generates the maximum deflection d_m.

5.1. Linearised theory

For small fan angles α, we can linearise the expressions derived in Section 3 to find, from (3.12), that the half-contact width and the scaled load and reaction forces are

$$\ell(\alpha) = W^*(\alpha) = (R_0 + h)\pi\alpha/2, \qquad X^*(\alpha) = (R_0 + h)\alpha, \tag{5.3}$$

and the corresponding deflection is

$$d(\alpha) = \tfrac{1}{8}(R_0 + h)(\pi^2 - 4)\alpha. \tag{5.4}$$

If α varies over the range $0 \leqslant \alpha \leqslant \alpha_m$ then the maximum deflection is

$$d_m = \tfrac{1}{8}(R_0 + h)(\pi^2 - 4)\alpha_m. \tag{5.5}$$

The parametric relation between the distance x from the centre line and the fan angle parameter α is given by solving (5.1) for x, so that

$$x^2 = (R_W + R_0 - d(\alpha))^2 - (R_W + R_0 - d_m)^2, \tag{5.6}$$

which, for small deflections reduces to

$$x^2 = 2(R_W + R_0)(d_m - d(\alpha)) = (R_W + R_0)(R_0 + h)\tfrac{1}{4}(\pi^2 - 4)(\alpha_m - \alpha), \tag{5.7}$$

with the maximum distance equal to

$$x_m = \{(R_W + R_0)(R_0 + h)\tfrac{1}{4}(\pi^2 - 4)\alpha_m\}^{1/2}. \tag{5.8}$$

Since the half-width of the contact region is $\ell = (R_0 + h)\pi\alpha/2$, the shape of the contact region is given by elimination of α between (5.7), (5.8) and (5.3) yielding

$$(R_W + R_0)(\pi/2 - 2/\pi)\ell = x_m^2 - x^2. \tag{5.9}$$

The (linearised) contact region is shown by the dashed lines on Figure 14, when $R_W = 2R_0$.

The total load carried by the contact region is given by (see Figure 13).

$$\mathrm{F} = 4\int_{x=0}^{x=x_m} G^* W^*\{\alpha(x)\}\cos(\theta)\mathrm{d}x \tag{5.10}$$

$$= 2G^*(R_0 + h)\pi \int_{\alpha=0}^{\alpha=\alpha_m} \alpha\left(-\frac{\mathrm{d}x}{\mathrm{d}\alpha}\right)\cos\,\theta\,\mathrm{d}\alpha, \tag{5.11}$$

where $\cos\,\theta = (1 - k\alpha_m)/(1 - k\alpha)$ and $k = \frac{1}{8}(R_0 + h)(\pi^2 - 4)/(R_W + R_0)$. Within the confines of the linear theory the $\cos\,\theta$ term can be taken to be equal to 1. Since the relation between x and α is defined in (5.7) this reduces to the integral

$$\mathrm{F} = \tfrac{1}{2}G^*(R_0 + h)\pi[(R_W + R_0)(\pi^2 - 4)]^{1/2}\int_0^{\alpha_m} \frac{\alpha}{(\alpha_m - \alpha)^{1/2}}\,\mathrm{d}\alpha$$

$$= \tfrac{2}{3}\,\mathrm{G}^*(R_0 + h)\pi[(R_W + R_0)(R_0 + h)(\pi^2 - 4)]^{1/2}\alpha_m^{3/2}. \tag{5.12}$$

Hence, in terms of the maximum deflection d_m, the overall force-deflection relation for the tyre becomes

$$\mathrm{F} = \frac{32\sqrt{2}}{3}\left(\frac{\pi}{\pi^2 - 4}\right)G\,\log\left(1 + \frac{h}{R}\right)(R_W + R_0)^{1/2}d_m^{3/2}. \tag{5.13}$$

This load-deflection relation is reminiscent of the relation

$$\mathrm{F} = \frac{16}{3}GR^{1/2}d^{3/2} \tag{5.14}$$

for contact between a sphere of radius R of incompressible material and a rigid plane, which may be derived from the Hertz theory of contact. In fact (5.13) implies that the force is approximately $1{\cdot}5\log(1 + h/R_0)$ times the Hertz theory result.

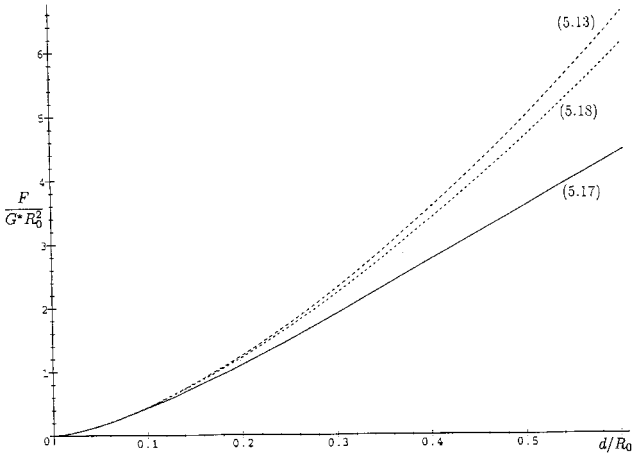

Figure 15. The load-deflection relations for the tyre. The loads are scaled by $G^*R_0^2$ and the deflection by R_0.

5.2. NONLINEAR RESULTS

We can adopt the same procedures for the parametric analysis derived in Section 3. If we let α range over the interval $0 \leqslant \alpha \leqslant \alpha_m$, the half contact length $\ell(\alpha)$, the scaled load $W^*(\alpha)$, reaction $X^*(\alpha)$ and the deflection $d(\alpha)$ are specified by (3.10), (3.12) and (3.14). The maximum deflection is given by $d_m = d(\alpha_m)$. The shape of the contact region is specified parametrically by the half-width $\ell(\alpha)$, from (3.10), which occurs at the distance

$$x = x(\alpha) = [(R_W + R_0 - d(\alpha))^2 - (R_W + R_0 - d(\alpha_m))^2]^{1/2} \tag{5.15}$$

from the centre line. The shape of the contact region (for the same value of the maximum deformation $d_m = 0{\cdot}3R_0$ where $R_W = 2R_0$) is shown on Figure 14, where it is compared with the linearised theory.

The total load can be expressed as an integral over the contact region in the form

$$\mathrm{F} = 4\int_0^{x_m} G^*W^*\cos(\theta)\,\mathrm{d}x. \tag{5.16}$$

Since we know W^* as a function of the deflection $d(\alpha) = D$, then $W^*(\alpha) = \overline{W}(D)$ for each cross-section and we can write this integral in the form

$$\begin{aligned}\mathrm{F} &= -4G^*\int_{D=0}^{D=dm}\overline{W}(D)\frac{R_W + R_0 - d_m}{R_W + R_0 - D}\frac{\mathrm{d}x}{\mathrm{d}D}\,\mathrm{d}D \\ &= 4G^*\int_{D=0}^{D=dm} x(D)\frac{\mathrm{d}}{\mathrm{d}D}\left\{\overline{W}(D)\frac{R_W + R_0 - d_m}{R_W + R_0 - D}\right\}\mathrm{d}D.\end{aligned} \tag{5.17}$$

The second integral has been obtained by integration by parts. The differentiated expression in the second integral is reasonably linear, so that we can approximate this expression by $4\pi D/(\pi^2 - 4)$ from the linear relations. Given the form (5.15) for x as a function of $D(= d_t(x))$ this integral can be evaluated and a second approximate load-deflection curve can be found for the tyre. It is

$$\mathrm{F} = \frac{8\pi G^*}{(\pi^2 - 4)}\left[a(a^2 - z^2)^{1/2} - z^2\log\left(\frac{a + (a^2 - z^2)^{1/2}}{z}\right)\right], \tag{5.18}$$

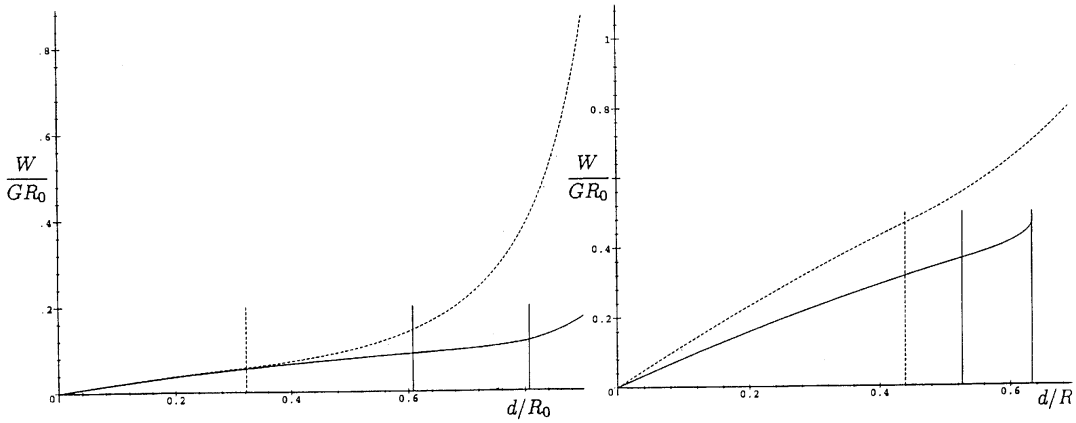

Figure 16. The Load W/GR_0 as a function of the deflection d/R_0. (a) $h/R_0 = 0{\cdot}1$; (b) $h/R_0 = 0{\cdot}5$; Hill's results ------- present results ——.

where $a = R_W + R_0$, $z = R_W + R_0 - d_m$.

The numerical evaluation of the integral (5.17) is also possible. The two approximate load-deflection curves for the tyre and the exact one are given on Figure 15. The highest curve corresponds to the linear approximation (5.13), the next is (5.18) and the lowest curve is the numerical evaluation of (5.17). It will be noticed that even the linearised form (5.13) gives a reasonable approximation when the deflections are less than $0{\cdot}2R_0$.

6. Discussion

This paper concerns the plane-strain deformation of a fibre-reinforced shell with a semicircular cross-section. The circumferential reinforcement makes the material highly anisotropic and the deformations are assumed to be large. The idealisations that the fibres are inextensible, continuously distributed through the material, and that it is incompressible permit a straightforward solution to the problem. It is of interest to note that for sufficiently large deformations a central fan is generated whose position and fan angle is determined by the solution and change as the deformation increases. To the author's knowledge this is the first time such a 'free' fan has been found in this field.

The initial impetus to examine this problem arose from discussions on finite deformations of cylindrical shells with Professor J. M. Hill, see Hill [21], [22] and [23]. Hill [23] has found an approximate solution to this problem by taking an exact finite plane-strain deformation of a thick semi-circular shell consisting of a Mooney–Rivlin material. The constants in his solution are used to balance the resultant forces applied across the curved surfaces rather than the exact stress or displacement boundary conditions which apply at each point of the curved surfaces. The Mooney–Rivlin material is an incompressible and isotropic material with the shear modulus $G = 2(C_1 + C_2)$ and the deformation field used by Hill is rather different from the exact solution which has been derived for the idealised circumferentially reinforced material discussed here. Figure 16 gives a comparison between the overall load-deflection relation derived by Hill ([23], Equation 4.16) and that deduced in this paper. A surprisingly good measure of agreement is achieved for thin shells ($h/R_0 = 0{\cdot}1$) with the approximate Mooney–Rivlin solution predicting a stiffer shell than the fibre-reinforced one when

$h/R_0 = 0{\cdot}5$. The point at which the form of Hill's solution changes and the central fan and upper fan regions in the present solution are denoted by vertical lines.

The solutions found by Hill are largely buckled solutions. The question of whether the ideal theory could predict the buckling of a shell has not been addressed in this paper. Following the work of Hill (see [22, 23]) one might expect the centre line CC′ (see Figure 2b) to move down and the point C′ to separate from the indentor in a buckled configuration. However, this configuration can only be achieved by the outer surface C′B′ sliding along PP′ and, if frictional forces are set up between C′B′ and PP′, it seems unlikely that the resultant reaction force will be sufficiently great to maintain a buckled region. If, however, the surfaces are smooth, then the reaction force may be sufficiently large to buckle the section BCC′B′ in the manner suggested by Pipkin and Kao [24]. This question requires further investigation. The extension of this work to incorporate the effects of internal pressure, a non-semicircular cross-section, and transverse forces, with the possibility that these idealised solutions may provide a relatively straightforward method for evaluating the approximate deformation field in a vehicle tyre will be examined in a future paper.

Acknowledgements

The author would like to record his thanks to Professor J. M. Hill for a very interesting study period at the University of Wollongong during the summer of 1997.

It is with much pleasure that I record my best wishes to Professor Tony Spencer on his seventieth birthday. As a colleague for the past thirty-seven years, I am indebted to him scientifically and socially in ways too numerous to mention!

References

1. A. J. M. Spencer, *Deformations of Fibre-Reinforced Materials*. London: Oxford University Press (1972) 128pp.
2. J. F. Mulhern, T. G. Rogers and A. J. M. Spencer, A continuum model for fibre-reinforced plastic materials. *Proc. R. Soc. Lond* A301 (1967) 473–492.
3. A. C. Pipkin, and T. G. Rogers, Plane deformations of incompressible fibre-reinforced materials. *J. Appl. Mech.* 38 (1971) 634–640.
4. A. C. Pipkin, Finite deformations of ideal fibre-reinforced composites. In: G. P. Sendeckyj (ed.), *Composite Materials, Vol 2: Micromechanics*. New York: Academic Press (1974) pp. 251–308.
5. T. G. Rogers, Finite plane deformations of strongly anisotropic materials. In: Hutton, Pearson and Walters (eds.), *Theoretical Rheology*. London: Applied Science Publishers (1975) pp. 141–168.
6. A. J. M. Spencer (ed.), *Continuum Theory of the Mechanics of Fibre-Reinforced Composites*. Wien–New York: Springer-Verlag (1984) 284 pp.
7. I. D. R. Bradford, A. H. England and T. G. Rogers, Finite deformations of a fibre-reinforced cantilever; point force solutions. *Acta Mechanica* 91 (1992) 77–95.
8. A. H. England, T. G. Rogers and I. D. R. Bradford, Finite deformations of a fibre-reinforced cantilever: Distributed-load solutions. *Q. J. Mech. Appl. Math.* 45 (1992) 711–732.
9. A. H. England and T. G. Rogers, Loading and unloading of an elastic-plastic fibre-reinforced cantilever. *Mech. Res. Comm.* 19 (1992) 333–340.
10. A. H. England, T. G. Rogers and P. W. Gregory, Reverse plastic yield in the unloading of highly anisotropic elastic-plastic cantilevers. *Materials Science Forum* 123–125 (1993) 215–224.
11. A. H. England, P. W. Gregory and T. G. Rogers, Finite elastic-plastic deformations of an ideal fibre-reinforced beam bent around a cylinder. *Z. angew. Math. Phys.* 46 (1995) 401–426.
12. T. G. Rogers, I. D. R. Bradford and A. H. England, Finite plane deformations of highly anisotropic elastic-plastic plates and shells. *J. Mech. Phys. Solids* 40 (1992) 1595–1606.

13. P. W. Gregory, T. G. Rogers and A. H. England, Loading and unloading of highly anisotropic elastic-plastic beams. *J. Mech. Phys. Solids* 42 (1994) 1019–1046.
14. L. R. G. Treloar, *The Physics of Rubber Elasticity*. Oxford: University Press (1958) 310 pp.
15. M. Nakajima and M. Kurashige, Finite plane deformation of an ideal fibre-reinforced material (experimental examination). *Japan Soc. Mech. Eng. Int. J.* 32 (1989) 396–402.
16. T. G. Rogers and A. C. Pipkin, Finite lateral compression of a fibre-reinforced tube. *Q. J. Mech. Appl. Math.* 24 (1971) 311–330.
17. A. H. England and P. W. Gregory, Finite lateral compression of an elastic-plastic fibre-reinforced tube: Loading solutions. *J. Mech. Phys. Solids* 47 (1999) 371–395.
18. A. C. Pipkin, Energy changes in ideal fibre-reinforced composites. *Q. Appl. Math.* 35 (1978) 455–463.
19. T. French, *Tyre Technology*. Bristol and New York: Adam Hilger (1989) 170 pp.
20. S. K. Clark, *Mechanics of Pneumatic Tyres*. Washington: U.S. Department of Transport (Ref HS 805 952) (1981) 931 pp.
21. J. M. Hill and D. J. Arrigo, Transformations and equation reductions in finite elasticity I: Plain strain deformations. *Math. Mech. Solids* 1 (1996) 155–175.
22. J. M. Hill, Buckling of long thick-walled circular cylindrical shells of isotropic incompressible hyperelastic materials under uniform external pressure. *J. Mech. Phys. Solids* 23 (1975) 99–112.
23. J. M. Hill, An approximate load-deflection relation for a long half-cylindrical tube compressed between parallel plates. *Z. angew. Math. Phys.* 28 (1977) 169–175.
24. B. C. Kao and A. C. Pipkin, Finite buckling of fibre-reinforced columns. *Acta Mech.* 13 (1972) 265–280.